In vivo bladder imaging with microelectromechanical-systems-based endoscopic spectral domain optical coherence tomography

Zhenguo Wang
State University of New York at Stony Brook
Department of Biomedical Engineering
Stony Brook, New York 11794

Christopher S. D. Lee
Wayne C. Waltzer
State University of New York at Stony Brook
Department of Urology
Stony Brook, New York 11794

Jingxuan Liu
State University of New York at Stony Brook
Department of Pathology
Stony Brook, New York 11794

Huikai Xie
University of Florida
Electrical and Computer Engineering Department
Gainesville, Florida 32611

Zhijia Yuan
Yingtian Pan
State University of New York at Stony Brook
Department of Biomedical Engineering
Stony Brook, New York 11794
E-mail: yingtian.pan@sunysb.edu

Abstract. We report the recent technical improvements in our microelectromechanical systems (MEMS)-based spectral-domain endoscopic OCT (SDEOCT) and applications for *in vivo* bladder imaging diagnosis. With the technical advances in MEMS mirror fabrication and endoscopic light coupling methods, the new SDEOCT system is able to visualize morphological details of the urinary bladder with high image fidelity close to bench-top OCT (e.g., 10 μm/12 μm axial/lateral resolutions, >108 dB dynamic range) at a fourfold to eightfold improved frame rate. An *in vivo* animal study based on a porcine acute inflammation model following protamine sulfate instillation is performed to further evaluate the utility of SDEOCT system to delineate bladder morphology and inflammatory lesions as well as to detect subsurface blood flow. In addition, a preliminary clinical study is performed to identify the morphological features pertinent to bladder cancer diagnosis, including loss of boundary or image contrast between urothelium and the underlying layers, heterogeneous patterns in the cancerous urothelium, and margin between normal and bladder cancers. The results of a human study (91% sensitivity, 80% specificity) suggest that SDEOCT enables a high-resolution cross-sectional image of human bladder structures to detect transitional cell carcinomas (TCC); however, due to reduced imaging depth of SDEOCT in cancerous lesions, staging of bladder cancers may be limited to T1 to T2a (prior to muscle invasion). [DOI: 10.1117/1.2749744]

Keywords: optical coherence tomography; bladder cancer diagnosis; spectral domain; microelectromechanical systems; endoscopy.

Paper 06329R received Nov. 15, 2006; revised manuscript received Jan. 26, 2007; accepted for publication Jan. 29, 2007; published online Jul. 3, 2007.

1 Introduction

Bladder cancer is among the most frequent types of malignancy and one of the leading causes of death in the United States, with estimated 61,420 new cases diagnosed and 13,060 deaths in 2006 (Ref. 1). Most bladder cancers are superficial carcinomas and originate in the basal cell layer of the urothelium. Thus, early diagnosis is crucial for appropriate treatment and enables enhancement of the cure rate and survival of patients. Yet this remains a clinical challenge. For instance, screening techniques such as cytology,[2] fluorescence *in situ* hybridization,[3] and bladder tumor antigen (BTA) (Ref. 4), are very sensitive for clinical detection of carcinoma *in situ* (CIS) and high-grade transitional cell carcinomas (TCCs); however, these techniques are much less sensitive for the early diagnosis of low-grade TCCs and are unable to locate the cancerous lesions, which compromises their ultimate effectiveness. On the other hand, conventional medical imaging methods such as x-ray, computed tomography (CT), and magnetic resonance imaging (MRI) fail to detect early bladder malignancies because of their resolution limitation. As a result, cystoscopy remains the current clinical standard for early bladder cancer detection. However, as cystoscopy is an *en face* imaging modality and provides only surface imaging without displaying any morphological details below the bladder surface, it often misses flat early bladder cancers such as CIS that may be visually normal or unspecific; thus, random biopsy is necessary for conclusive diagnosis and staging of malignancy for patients with positive findings in urine cytology. However, this invasive procedure may still miss approximately 50% of early flat bladder cancers.[5,6] Therefore, a noninvasive and high-resolution imaging technique would be highly desirable to improve the diagnostic sensitivity and specificity, critical to the therapeutic benefits of early bladder cancer patients.

Recent advances in optical imaging have demonstrated a number of potential modalities for early bladder cancer detection. For instance, fluorescence cystoscopy following photo-

Address all correspondence to: Yingtian Pan, PhD, Associate Professor, State University of New York at Stony Brook, Department of Biomedical Engineering, Stony Brook, New York 11794-8181; Tel: 631-444-1451; Fax: 631-444-6646; Email: yingtian.pan@sunysb.edu

1083-3668/2007/12(3)/034009/8/$25.00 © 2007 SPIE

sensitizer administration has significantly enhanced diagnostic sensitivity by detecting[7,8] photochemical changes pertinent to TCCs. Optical coherence tomography (OCT), on the other hand, can provide high-resolution cross-sectional images of bladder morphology at a depth of 1 to 2 mm, which is advantageous for detection of various types of superficial lesions.[9–11] Recent technological advances of spectral domain OCT (SDOCT) has dramatically improved the dynamic range and imaging rate.[12,13] With optical configurations in spectral domain that circumvent the slow mechanical scanning in the reference arm, imaging rate has been improved up to several hundredfold and potentially enables *in vivo* 3-D OCT imaging.[14–16] In addition, direct access of spectral interference modulation enables Fourier-domain Doppler OCT (FDOTC) for real-time blood flow imaging,[17,18] ultra-high-resolution FDOCT (Refs. 17 and 19) of retinal imaging, polarization-sensitive SDOCT (Refs. 20 and 21), and spectral second-harmonic generation[22] OCT to enhance image contrast in biological tissue. In addition to technological advances, clinical applications of SDOCT have already been performed in various tissues, including eye,[15] esophagus,[14] and urinary bladder,[23] demonstrating dramatic improvement on image fidelity and imaging rate.

In terms of bladder imaging, OCT has demonstrated the great potential to diagnose various bladder diseases, especially bladder cancer.[10,24–29] Implementations of OCT endoscopes using a rotary joint, piezoelectric transducer (PZT), paired-angle-rotation-scanning probe and microelectromechanical system (MEMS) micromirror have been reported[30–32] for *in vivo* imaging diagnosis of urinary bladder cancers to fully take advantage of the OCT technique. Since the introduction of MEMS technology to OCT endoscopy,[31] we have recently made substantial improvements on the design and packaging of MEMS-based OCT endoscopes. Here, we demonstrate our recent technological advances on spectral-domain endoscopic OCT (SDEOCT) that enables faster structural imaging and simultaneous blood flow measurement of bladder *in vivo*. We compare the image results obtained from time-domain OCT (TDOCT) and SDOCT systems. Then, we present diagnostic results to evaluate the utility and potential limitations of SDEOCT for *in vivo* bladder imaging diagnosis based on animal and preliminary clinical studies.

2 Materials and Methods

2.1 *MEMS-Based SDEOCT*

As depicted in Fig. 1, a high-power broadband source (BBS) is employed, which can provide pigtailed output power of 12 mW at central wavelength of $\lambda=1320$ nm and with full width half maximum spectral bandwidth of $\Delta\lambda=78$ nm (resulting in a coherence length $L_C \approx 10\ \mu$m). The light is delivered to a fiber optic Michelson interferometer in which light is divided equally to reference and sample arms. For visual guidance, the red light from a 670-nm diode laser is coupled into the input arm via a 95%:5% fiber coupler.

In contrast to TDOCT, which uses a grating-lens-based optical delay line to implement longitudinal scan, a stationary mirror is employed in the reference arm to match the optical path lengths between the sample and the reference arms of the fiber optic interferometer. The sample arm can be either connected to a bench-top stereoscope in which light exiting the

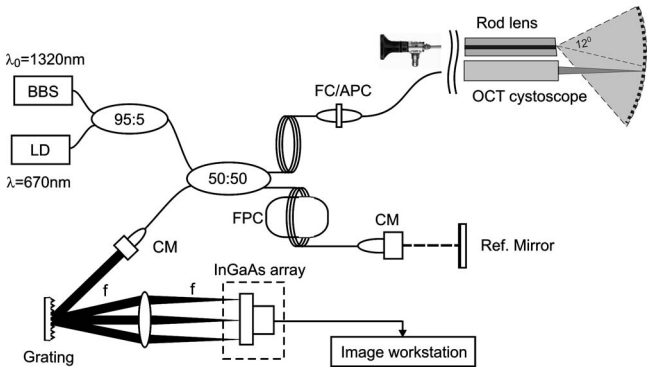

Fig. 1 Schematic diagram of a fiber-optic SDEOCT system. The SDOCT system is connected to a MEMS-based OCT endoscope for *in vivo* bladder imaging study: BBS, broadband source ($\lambda_0=1320$ nm, $\Delta\lambda_{FWHM}=78$ nm, $P=12$ mW); LD, aiming laser diode ($\lambda=670$ nm); CM, fiber optic collimator; FPC, fiber polarization controller. For the endoscopic setup, lateral scanning range is up to 4.5 mm, and the spatial resolutions are 10 μm axially and 12 μm laterally. The single-frame dynamic range of the endoscopic OCT system reached 108 dB. A rod lens imaging catheter is placed parallel to OCT cystoscope for image guidance.

fiber is collimated to ϕ4.5 mm, scanned laterally by a servomirror, and focused by an $f=40$ mm achromatic lens onto biological tissue under examination. Through a modified FC/APC (fiber channel/angled physical contact) connector, it can also be connected to a MEMS-based pigtailed OCT endoscope, which is inserted into the ϕ4 mm instrument channel of a 22Fr commercial endoscopic sheath for *in vivo* animal or human study. As previously reported,[31] the optical arrangement in the distal OCT scope enables visual guidance via a ϕ2.8-mm scope with either white light or fluorescence image of the bladder surface. In the OCT endoscope, the light from the single-mode (SM) fiber is coupled by a 0.25-pitch selfoc lens to a ϕ1.0-mm collimated beam, deflected by a fixed reflecting prism and a MEMS mirror, and is then focused by a laser doublet (f10 mm/ϕ5 mm) onto the bladder wall for OCT scan. The transverse light scanning in the OCT endoscope is facilitated by an Al-coated CMOS-MEMS mirror, which is actuated over 18° or 4.2 mm (limited by the scope size) in the transverse direction by an applied electrical voltage or current at a repetition rate up to 100 Hz.

In the detection fiber, the light beams returning from sample and reference arms are recombined and connected to a spectral radar in which light is collimated by a fiber optic achromatic lens ($f=55$ mm), diffracted by a holographic grating ($d=1200$ mm^{-1}), and then focused by an achromatic lens ($f=120$ mm) onto a 1024-pixel-line InGaAs photodiode array (Sensors Unlimited, New Jersey) mounted on a motored 3-D stage for high-precision focusing alignment. The detected spectral graph, including spectrally encoded interference fringes from different depth within the biological sample, is amplified and then digitized and streamlined to the hard disk of an image workstation via a multi-channel 12-bit analog-to-digital converter (A/D) (DAQ6111E, NI) at 5 MHz to enable 2-D imaging at nearly 8 fps (frames per second; post image processing). Because of complex data processing [e.g., spline interpolation, fast Fourier transform (FFT)] involved in converting spectral graphs to a reconstructed OCT image, instan-

taneous image processing and display is reduced to approximately 5 fps, but is sufficient for *in vivo* visualization of bladder wall. Data processing to reconstruct each depth profile or A-scan is implemented simultaneously with scanning of the lateral servo mirror, i.e., the MEMS mirror in the OCT endoscope following detection of each spectral graph until a 2-D image is completed and displayed. Similar to TDEOCT, the axial and the transverse resolutions of SDEOCT are determined by the coherence length L_c and the focal spot size of the OCT scope, respectively. Based on the preceding parameters used in our setup, the axial resolution is $\sim 10\ \mu$m, and the transverse resolution is $\sim 12\ \mu$m.

In terms of SDOCT versus TDOCT, of particular interest is the ability of SDOCT to simultaneously image tissue architecture and subsurface blood flow/velocity (i.e., Doppler SDOCT) in nearly real time, which can be readily extracted from differential spectrograph data (i.e., phase difference) with minimal hardware modification.[17] Doppler OCT imaging can provide very useful functional blood flow information pertinent to bladder cancer because abnormal angiogenesis underneath the bladder surface can be induced by bladder tumorigenesis. For instance, cancer cells can induce abnormal angiogenesis once the tumor size is greater than 1 to 2 mm in diameter,[33] and when the fresh nutrients and oxygen are rapidly depleted and new blood vessel formation is necessary to replenish them.[34] Thus, detecting abnormal angiogenesis within bladder wall can provide additional diagnostic information for bladder cancers, thereby improving diagnostic sensitivity and specificity. As previously reported,[17] subsurface Doppler flow image can be acquired by subtraction of multiple (N) A-scans at each lateral position. In addition to the amplitude term $I(z)=|\tilde{I}(z)|$ of the inverse complex Fourier transform $\tilde{I}(z)=i\mathrm{FFT}[I(k)]$, which constitutes the structural SDOCT image, the phase term $\Phi(z,\tau)=\tan^{-1}\{\mathrm{Im}[\tilde{I}(z)]/\mathrm{Re}[\tilde{I}(z)]\}$ is extracted. And the phase variation between two adjacent A-scans at the same lateral position $\Delta\Phi(z,\tau)$ is used to reconstruct the Doppler flow velocity $v(z)=\Delta\Phi(z,\tau)\lambda/[4\pi\tau\cos(\alpha)]$ (Ref. 17), where τ is the interval between two A-scans. The excessive phase noise that imposes a major limitation to the dynamic range of Doppler OCT can be improved by implementing multiple scans and averaging[35] $\Delta\Phi(z,\tau)$. The major advantages of such technique for *in vivo* Doppler imaging are obvious: it does not require hardware modification and imaging can be much faster to reduce the influence of motion artifacts.

2.2 *Animal Model for In Vivo SDEOCT Study*

The animal model employed in this study has been reported previously;[23] therefore, only a brief summary is provided here. Because of lack of a large animal bladder cancer model suitable for testing OCT endoscopes for *in vivo* imaging, the porcine acute bladder inflammation model was modified based on a well-developed rat bladder irritation model. Protamine sulfate solution (15 mg/kg) was instilled intravesically into a female porcine bladder and retained inside for 30 to 45 min while the animal was under general anesthesia, then the instillation was curtailed and animal was freed to return to the cage. Cystoscopic OCT was performed 24 to 48 h after the instillation, enabling us to examine the utility of this technique in imaging the morphological changes resulting from acute bladder irritation due to exposure to protamine sulfate. Acute responses included disruption to the urothelium or urothelial denudation and acute inflammatory lesions such as edema, vasodilatation, and sometimes acute cystitis. Although it did not induce bladder cancer growth, this bladder irritation model provided a controllable mechanism to examine endoscopic OCT technology in identifying various morphological changes associated with acute inflammation, i.e., noncancerous lesions. Prior to OCT imaging, the pig was anesthetized with 5% inhaled isoflurane for induction and 1 to 2.5% for maintenance, then the bladder was imaged by white-light-guided OCT inserted into a standard 22Fr cystoscopic sheath. The entire imaging procedure lasted less than 30 min, and then the anesthesia was curtailed and the animal was freed. Human study was performed on patients who were scheduled to undergo cystoscopic procedures for bladder cancer diagnosis and treatment in the operating room and had consented for add-on cystoscopic OCT, and the entire OCT imaging procedure lasted less than 10 min. All the animal and human studies followed the protocols approved by the Institutional Animal Care and Use Committee (IACUC) and Institutional Review Board (IRB) committees of the State University of New York (SUNY) at Stony Brook.

3 Results

To examine the imaging fidelity and suitability of MEMS-based OCT systems for *in vivo* bladder imaging, we performed experiments to compare endoscopic versus bench-top OCT systems and endoscopic SDOCT versus TDOCT systems. The axial resolution of the bench-top OCT setup that employed a ϕ4.5 mm beam collimator and a $f/40$ mm achromatic lens was approximately $\phi 12\ \mu$m, equivalent to that of the MEMS-based endoscopic OCT catheter with a ϕ1 mm beam collimator and a $f/10$ mm achromatic lens. But the transverse laser steering range of OCT catheter was limited ($<$4.6 mm) by the scope size and was smaller than that of the bench-top setup (6 mm). Figure 2 shows the comparative 2-D cross-sectional OCT images of a porcine bladder taken by OCT endoscope [Fig. 2(A)] versus bench-top OCT stereoscope [Fig. 2(B)]. The morphological details of porcine bladder (a close mammalian homologue) such as urothelium (U), lamina propria (LP), and muscularis (M) in Fig. 2(A) were clearly delineated at fairly comparable image fidelity to those in Fig. 2(B), except for a slight reduction (2.87 dB) of image SNR due to light coupling loss in the endoscope. The result demonstrates the drastic improvement on our implementation of MEMS-based OCT catheter and justifies the utilities of *in vivo* bladder imaging study. Figure 3 shows the comparison between TDOCT and SDOCT endoscopic images. Both OCT images delineate the bladder morphology, e.g., U, LP, and M; however, a quantitative analysis between these two images indicates that at almost sixfold improved imaging rate, SDOCT [Fig. 3(B)] still shows a 2.5-dB enhanced image SNR compared with TDOCT [Fig. 3(A)]. Therefore, SDOCT offers benefits in both image fidelity and imaging speed for endoscopic *in vivo* imaging study. More importantly, SDOCT can provide simultaneous Doppler image to map subsurface blood flow distribution. For instance, Fig. 4 shows the result of calibration study using tissue phantom in which the profile

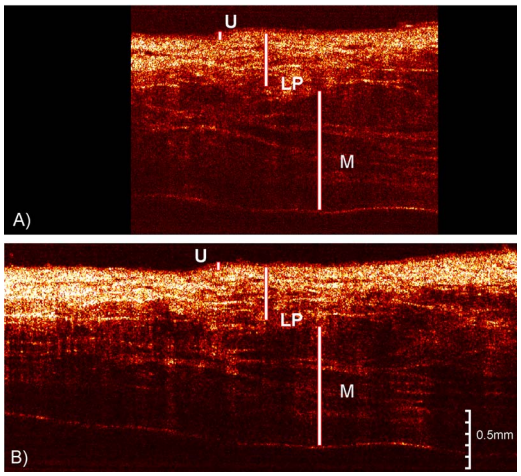

Fig. 2 Comparison between (A) cystoscopic OCT image and (B) bench-top OCT image of a fresh porcine bladder: U, urothelium; LP, lamina propria; M, muscularis. Image sizes: (A) 2 mm axially × 4.2 mm laterally; (B) 2 mm axially × 6 mm laterally. Due to light coupling loss in the endoscope, there is a slight SNR reduction (~2.87 dB) in image (A).

of two bidirectional flows (1% intralipid solution, $\mu_s \approx 2.4\ \mathrm{cm}^{-1}$) in a ϕ0.56-mm translucent conduit can be quantitatively imaged by SDOCT. Based on the calibration result, Fig. 5 shows the result of *in vivo* porcine bladder study in which two minute blood flows (roughly ϕ150 μm) in the lamina propria (about 800 μm underneath the bladder surface) were detectable, as indicated by the dashed circles with estimated apparent flow rates of 0.51 and 0.13 mm/s. It was observed during the experiment that the phase noise induced by bladder movement and handshaking compromised the dynamic range of *in vivo* blood flow imaging. Currently, we are implementing interpixel-shifted SDOCT[36] to increase imaging rate (while maintaining imaging depth) and thus to minimize the influence of motion artifacts on Doppler OCT *in vivo*.

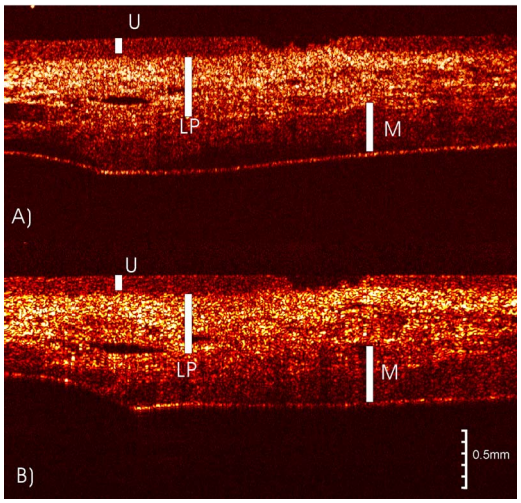

Fig. 3 Comparison between (A) cystoscopic TDOCT and (B) SDOCT bladder images: U, urothelium; LP, lamina propria; M, muscularis. Image size: 2 mm axially × 4.2 mm laterally. (B) shows 2.5 dB enhanced image SNR compared with (A) at ~6 times faster frame rate.

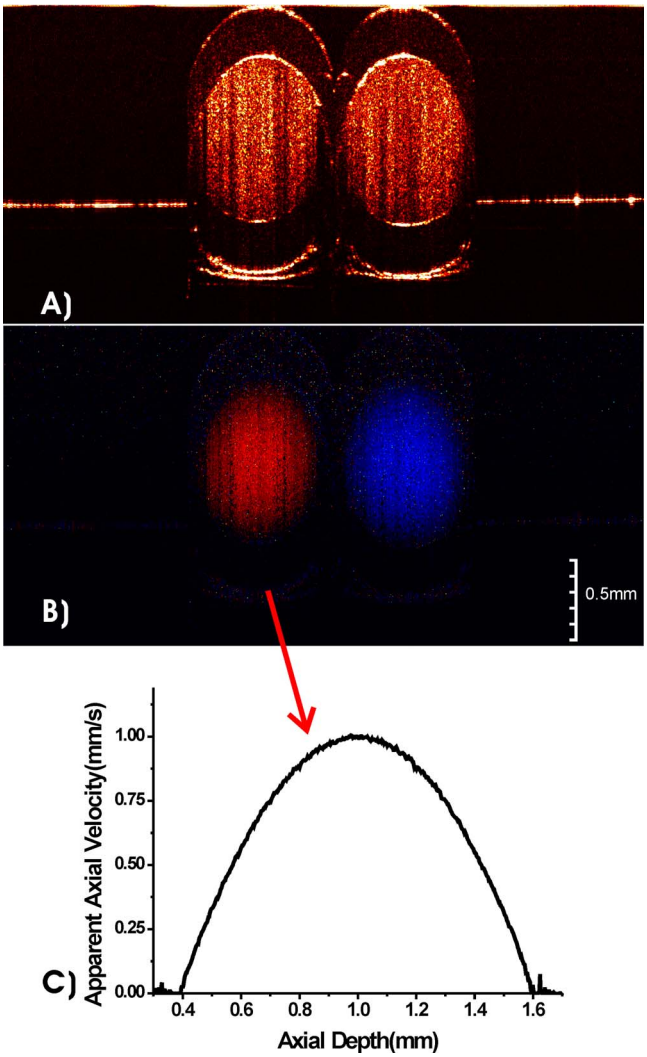

Fig. 4 2-D Doppler OCT of bidirectional flows of intralipid solution: (A) structural image, (B) flow image, and (C) depth-dependent mean flow rate. Using parabolic curve fitting, the measured apparent volumetric velocity is ~3.1 ml/h, which is consistent with experimental flow set of 3.0 ml/h (the slant angle was 20 deg and the camera frame rate 7.7 kHz).

Following successful *in vivo* porcine bladder imaging study, we initiated *in vivo* clinical study on symptomatic patients scheduled for operation-room examinations and treatments such as cystoscopy with possible biopsies, transurethral resection of bladder tumors (TURBT), and cystectomy. As a blind study to examine the diagnostic sensitivity and specificity of OCT cystoscopy, the OCT diagnosis was given during the cystoscopic procedure, and was later validated by the result of biopsied histology, which served as the gold standard of clinical diagnosis. Figure 6 shows the results for a normal human bladder, where Fig. 6(A) shows the surface image *in vivo*, Fig. 6(B) shows the endoscopic OCT image *in vivo*, and Fig. 6(C) shows the corresponding hematoxylin and eosin (H&E) stained histological section from the biopsied specimen. As we can see, the white light cystoscopic image with a field of view of approximately ϕ12 mm appears flat and uniform with plenty of visible subsurface blood vessels. Both

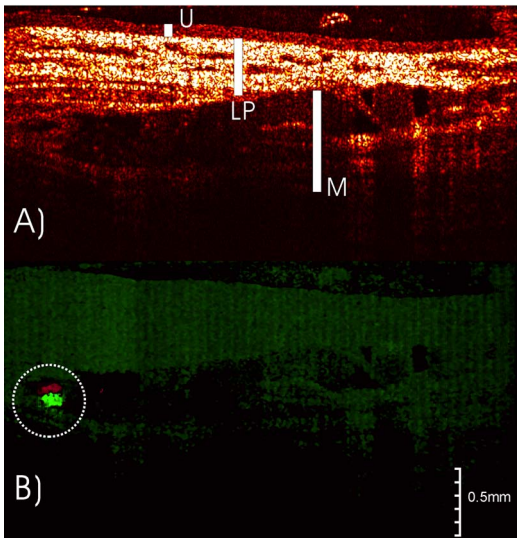

Fig. 5 Doppler SDEOCT of subsurface blood flow in a porcine bladder *in vivo*: U, urothelium; LP, lamina propria; M, muscularis. Image size: 2 mm axially × 4.2 mm laterally. Two-minute blood flows (roughly ϕ150 μm) were detected in the lamina propria (about 800 μm underneath the bladder surface). The estimated apparent flow rates were 0.51 and 0.13 mm/s, respectively.

endoscopic OCT and histological sections are 4.2 mm in the transverse direction and 2 mm in the vertical direction. It is obvious that the human bladder bears a close similarity to porcine bladder (Fig. 2) in terms of the anatomic architecture and optical properties such as scattering and absorption. The morphological details of normal human bladder delineated by OCT, e.g., the low-scattering urothelium, U; the high-scattering lamina propria, LP; and the upper muscularis, M correlated well with those in the histological section. For instance, the *in vivo* OCT measurement of urothelial thickness of d_U=67.9±5.6 μm matches the histological evaluation of d_U=62.8±4.1 μm, which appears as a homogeneous, low-scattering thin layer. In addition to normal bladder, Fig. 7 shows the result of a bladder tumor, including the transition to the adjacent normal bladder. The papillary appearance of the lesion is apparent under the cystoscopic surface RGB image as seen in Fig. 7(A). The OCT in Fig. 7(B) diagnoses the lesion as papillary TCC and clearly provides the margin between the tumor and the adjacent normal bladder wall. Unlike normal bladder in Fig. 6, the distinct morphological structures such as U, SM, and M were drastically changed: the urothelium was no longer distinguishable from underlying laminar propria due to carcinogenesis in the urothelium and the resultant increase in scattering properties and homogeneity. Here, the OCT diagnosis of this TCC was based on identifying papillary features of the lesion such as the dark holes as highlighted by arrows in the thickened cancerous urothelium. Histology in Fig. 7(C) confirms the lesion as a papillary TCC (low grade I/III, stage T2). Note that although OCT can mark the boundary of the papillary lesion, as highlighted by the dashed line, it may not always be able to stage the invasion of cancer (e.g., >T2a) because of signal loss in the cancerous region. High attenuation of the OCT signal in cancerous lesions can be attributed by light loss due to increased homogeneity (such as papillary features) and enhanced subsurface vascularization.

4 Discussion

In summary, we report the technical improvement of MEMS-based OCT cystoscope to enable high-resolution imaging of bladder morphology (e.g., urothelium, lamina propria, and upper muscularis) and function (e.g., subsurface blood flows) noninvasively, and the preliminary results of *in vivo* clinical diagnosis of transitional cell cancers. To examine the utility of cystoscopic OCT for *in vivo* imaging and diagnosis of bladder morphology, functions, and malformations (e.g., TCCs), we proposed a protocol that incorporated conventional cystoscopy, cystoscopic OCT, and excisional biopsy to compare the diagnostic results for each lesion, in which histological evalu-

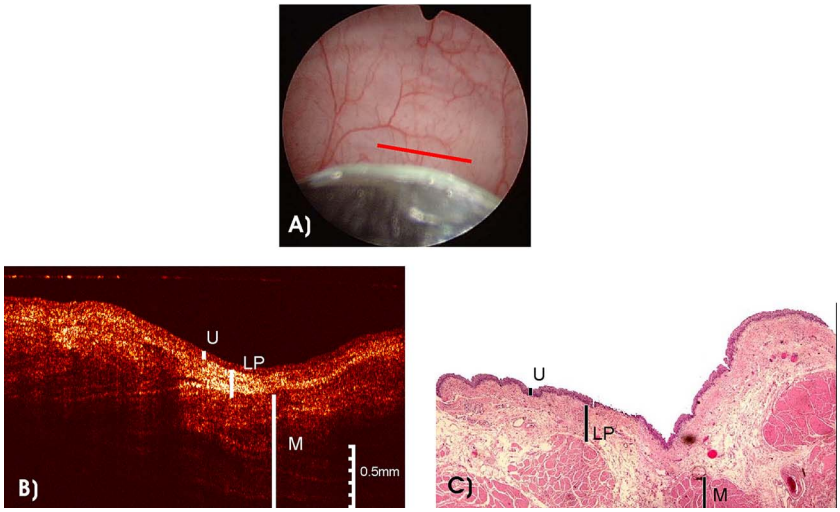

Fig. 6 Cystoscopic OCT image of a normal human bladder *in vivo*: (A) surface image, (B) cystoscopic OCT image, and (C) H&E stained histological section: U, urothelium; LP, lamina propria; M, muscularis. Image sizes for (A) and (B) are ϕ12 mm and 2 mm axially × 4.2 mm laterally, respectively. The red line in (A) indicates the lateral position of the OCT scan. (Color online only)

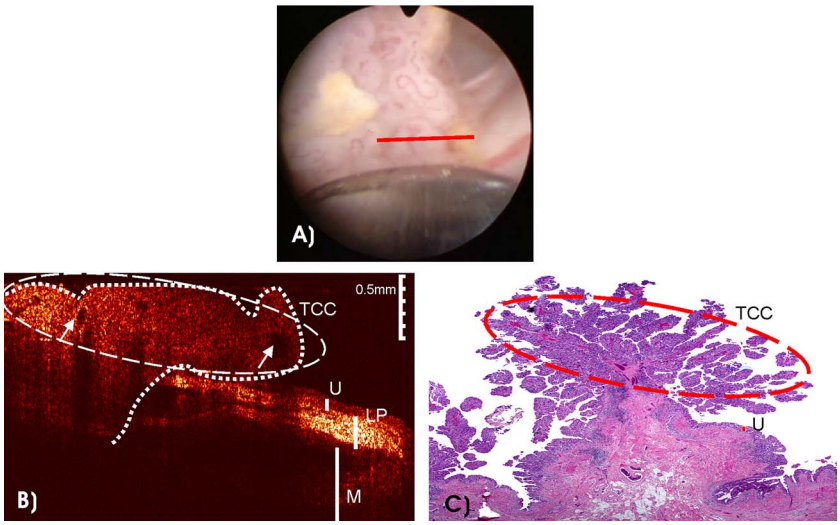

Fig. 7 Cystoscopic OCT image of a human bladder cancer *in vivo*: (A) surface image, (B) cystoscopic OCT image, and (C) H&E stained histological section: U, urothelium; LP, lamina propria; M, muscularis. Image sizes for (A) and (B) are ϕ12 mm and 2 mm axially × 4.2 mm laterally, respectively. The red line in (A) indicates the OCT scanning position. The cystoscopic OCT image clearly provides the margin between the tumor and the adjacent normal bladder wall, as indicated by the dash curve. The lesion shown is papillary TCC (low grade I/III, stage T2). (Color online only)

ation of the biopsied lesion specimens served as gold standard for clinical diagnoses. As the bladder surface images in Figs. 6(A) and 7(A) indicate, conventional cystoscopy is based on visual inspection of gross topological (i.e., superficial) changes of the bladder to diagnose bladder tumors. Therefore, it can efficiently locate and diagnose highly papillary TCCs as exemplified by Fig. 7. However, because of inability to resolve in depth direction, it is common that cystoscopy may fail to distinguish benign bladder inflammatory lesions from early flat TCCs such as CIS, both of which may show a normal or slightly reddish surface appearance.[37,38] Therefore, improved cystoscopic imaging techniques are required that will enable high-resolution visualization of morphological details below the bladder surface to diagnose early flat TCCs and to stage cancer invasion. Among several of the currently viable imaging techniques, OCT offers a great promise for noninvasive diagnosis of early bladder cancers, owing to its high spatial resolution (e.g., <10 μm at current stage) and high dynamic range (>100 dB) at imaging depths of 2 to 3 mm. Based on previous animal bladder carcinogenesis studies, the unique cross-sectional imaging fashion of OCT—which is an analog to histopathology—enables the urologist to visualize the morphological architectures of the bladder critical to early cancer diagnosis such as the urothelium, the lamina propria, and the upper muscularis noninvasively, instantaneously, and at resolution below 10 μm, close to histopathology, if implemented endoscopically.

Recently, there have been a number of reports on endoscopic OCT techniques; however, the development of a workable high-fidelity endoscopic OCT suitable for *in vivo* clinical imaging diagnosis remains a technical challenge. The MEMS-based OCT endoscope presented in this paper is of particular interest to urological applications for the following reasons. First, the larger beam size (e.g., $\geqslant\phi$1.0 mm) provides improved transverse OCT resolution (e.g., $\sim$12 μm). As we can see in Fig. 2, the cystoscopic OCT image quality is drastically enhanced to be comparable to bench-top OCT setup. Second, full-range MEMS laser scanning enables us to achieve a larger image size (e.g., $>$4.5 mm) in the transverse direction, which has been found very useful for precisely locating the cancer boundary, as shown in Fig. 7. Third, the front-view OCT catheter can be easily incorporated with surface imaging guidance for effective endoscopic OCT examination of larger areas, such as the bladder surface. This is critical, because urologist always wants to know the surface condition and the location of the lesions under examination, and the combined surface and OCT images can eliminate some false positive diagnoses by OCT such as scar or calcified lesions resulted from previous TURBT. Fourth, the unique setup that incorporates surface and OCT scopes makes it easy to focus during *in vivo* imaging and the OCT scope is reliable, sterilizable, and cost effective. Moreover, although the current OCT catheter is rigid, it can be easily modified to a flexible OCT catheter because only the 20 mm distal tip must be rigid. This modification may enable access to some areas of the bladder such as the bladder neck where the current rigid OCT catheter fails. As shown in Fig. 6, the morphological details of a normal human bladder are clearly delineated. In contrast to a normal bladder, the contrast and structural details in cancerous lesions, as exemplified in Fig. 7, are drastically reduced or diminished, and the effective imaging depth is decreased. Because of this, the use of endoscopic OCT for staging cancer invasion is likely to be limited to stages T1 or T2a (i.e., prior to muscle invasion). Previous systemic *ex vivo* rat bladder carcinogenesis studies revealed that OCT differentiated TCC from normal bladder and benign lesions such as inflammatory lesions and hyperplasia by detecting enhanced urothelial backscattering as a result of the increased nuclear-to-cytoplasmic ratio in TCCs. However, it has been found that some human TCCs may also show no obvious increase in backscattering, such as the lesions in Fig. 7. More detailed human data and analysis are required to study the relation between urothelial backscattering enhancement and cancer grading and staging. Fortunately, hyperplasia is far less com-

mon in human cases than in the animal carcinogenesis model following MNU installation, and the estimated diagnostic sensitivity and specificity based on initial human cases (20 cases so far) are over 91 and 80%, respectively. Currently, the identification of TCCs is based on abnormal changes in the urothelium such as the papillary features of TCCs, as exemplified in Fig. 7(B). Based on more human data analysis and classification, potential future approaches to further improve OCT diagnosis of human TCCs *in vivo* will include detection of local vascularization with endoscopic Doppler OCT, quantification of urothelial backscattering for TCC grading, and endoscopic ultra-high-resolution OCT for quantification of nuclear-to-cytoplasmic ratio. The initial results of endoscopic Doppler OCT, as shown in Fig. 5, are of great interest for future detection of elevated tumor vasculature. However, we have noticed that due to phase noise induced in *in vivo* imaging, the dynamic range for small flow mapping is compromised. We are addressing the issue by employing common path optical topology[39,40] to minimize the phase drift caused by motion artifacts induced by patient or the examining physician.

5 Conclusions

A SDEOCT imaging system was presented and its utility in bladder cancer diagnosis was examined *in vivo* based on porcine data and an initial clinical trial. Preliminary results demonstrate the potential of MEMS-based SDEOCT to provide the morphological details of porcine and human bladders such as the urothelium, the lamina propria, and the upper muscularis at a resolution and contrast comparable to TDEOCT and even the bench-top OCT system. The SDEOCT imaging system can provide cross-sectional OCT images of 2 mm in the depth direction and 4.5 mm in the transverse direction per scan at a frame rate of approximately 8 fps. The imaging system is fully automatic and incorporated with surface cystoscope for visual guidance and complimentary diagnosis with OCT scope. Additional *in vivo* results of blood flows in the lamina propria of bladder and clinical diagnosis of human TCCs were presented, suggesting that MEMS-based SDEOCT is a very promising optical biopsy technique for noninvasive and instantaneous imaging diagnosis of bladder diseases such as early diagnosis of bladder cancers.

Acknowledgment

This research is supported in part by the National Institutes of Health (NIH) Grant No. 2R01-DK059265 (YP) and Grant No. R01-DK068401 (YP, WC), and National Science Foundation (NSF) Grant No. BES0423557 (HX). The contributions of Dr. D. Schulsinger, Dr. H. Adler, Dr. J. Kim, Dr. A. Kirshenbaum, and Dr. A. Mishail to clinical study are acknowledged.

References

1. *Cancer Facts & Figures 2006* (2006) (cited April 9, 2006); available from http://www.cancer.org/downloads/STT/CAFF2006PWSecured.pdf.
2. R. S. Cajulis, G. K. Haines, D. Friashidvegi, K. McVary, and J. W. Bacus, "Cytology, flow-cytometry, image-analysis, and interphase cytogenetics by fluorescence *in situ* hybridization in the diagnosis of transitional-cell carcinoma in bladder washes—a comparative-study," *Diagn. Cytopathol* **13**(3), 214 (1995).
3. M. F. Sarosdy et al., "Clinical evaluation of a multi-target fluorescent *in situ* hybridization assay for detection of bladder cancer," *J. Urol. (Baltimore)* **168**(5), 1950 (2002).
4. H. Leyh et al., "Comparison of the BTA stat (TM) test with voided urine cytology and bladder wash cytology in the diagnosis and monitoring of bladder cancer," *Eur. Urol.* **35**(1), 52 (1999).
5. M. Kriegmair, R. Baumgartner, R. Knuchel, H. Stepp, F. Hofstadter, and A. Hostetter, "Detection of early bladder cancer by 5-aminolevulinic acid induced porphyrin fluorescence," *J. Urol. (Baltimore)* **155**(1), 105 (1996).
6. D. Zaak et al., "Quantification of 5-aminolevulinic acid induced fluorescence improves the specificity of bladder cancer detection," *J. Urol. (Baltimore)* **166**(5), 1665 (2001).
7. M. Kriegmair, D. Zaak, R. Knuechel, R. Baumgartner, and A. Hofstetter, "5-aminolevulinic acid-induced fluorescence endoscopy for the detection of lower urinary tract tumors," *Urol. Int.* **63**(1), 27 (1999).
8. D. Zaak et al., "Endoscopic detection of transitional cell carcinoma with 5-aminolevulinic acid: results of 1012 fluorescence endoscopies," *Urology* **57**(4), 690 (2001).
9. G. J. Tearney, M. E. Brezinski, B. E. Bouma, S. A. Boppart, C. Pitris, J. F. Southern, and J. G. Fujimoto, "*In vivo* endoscopic optical biopsy with optical coherence tomography," *Science* **276**(5321), 2037 (1997).
10. M. J. Manyak et al., "Evaluation of superficial bladder transitional-cell carcinoma by optical coherence tomography," *J. Endourol* **19**(5), 570–574 (2005).
11. T. Q. Xie, M. L. Zeidel, and Y. T. Pan, "Detection of tumorigenesis in urinary bladder with optical coherence tomography: optical characterization of morphological changes," *Opt. Express* **10**(24), 1431 (2002).
12. R. A. Leitgeb, L. Schmetterer, W. Drexler, A. F. Fercher, R. J. Zawadzki, and T. Bajraszewski, "Real-time assessment of retinal blood flow with ultrafast acquisition by color Doppler Fourier domain optical coherence tomography," *Opt. Express* **11**(23), 3116 (2003).
13. J. F. de Boer, B. Cense, B. H. Park, M. C. Pierce, G. J. Tearney, and B. E. Bouma, "Improved signal-to-noise ratio in spectral-domain compared with time-domain optical coherence tomography," *Opt. Lett.* **28**(21), 2067 (2003).
14. Y. Yasuno, T. Endo, S. Makita, G. Aoki, M. Itoh, and T. Yatagi, "Three-dimensional line-field Fourier domain optical coherence tomography for *in vivo* dermatological investigation," *J. Biomed. Opt.* **11**(1), 014014 (2006).
15. M. Wojtkowski, V. Srinivasan, J. G. Fujimoto, T. Ko, J. S. Schuman, A. Kowalczyk, and J. S. Duker, "Three-dimensional retinal imaging with high-speed ultrahigh-resolution optical coherence tomography," *Ophthalmology* **112**(10), 1734 (2005).
16. R. Huber, M. Wojtkowski, and J. G. Fujimoto, "Fourier domain mode locking (FDML): a new laser operating regime and applications for optical coherence tomography," *Opt. Express* **14**(8), 3225 (2006).
17. R. A. Leitgeb, L. Schmetterer, C. K. Hitzenberger, A. F. Fercher, F. Berisha, M. Wojtkowski, and T. Bajraszewski, "Real-time measurement of *in vitro* flow by Fourier-domain color Doppler optical coherence tomography," *Opt. Lett.* **29**(2), 171 (2004).
18. B. J. Vakoc, S. H. Yun, J. F. de Boer, G. J. Tearney, and B. E. Bouma, "Phase-resolved optical frequency domain imaging," *Opt. Express* **13**(14), 5483 (2005).
19. B. Cense and N. A. Nassif, "Ultrahigh-resolution high-speed retinal imaging using spectral-domain optical coherence tomography," *Opt. Express* **12**(11), 2435 (2004).
20. J. Zhang, W. G. Jung, J. S. Nelson, and Z. P. Chen, "Full range polarization-sensitive Fourier domain optical coherence tomography," *Opt. Express* **12**(24), 6033 (2004).
21. B. H. Park, M. C. Pierce, B. Cense, S. H. Yun, M. Mujat, G. J. Tearney, B. E. Bouma, and J. F. de Boer, "Real-time fiber-based multi-functional spectral-domain optical coherence tomography at 1.3 mu m," *Opt. Express* **13**(11), 3931 (2005).
22. M. V. Sarunic, B. E. Applegate, and J. A. Izatt, "Spectral domain second-harmonic optical coherence tomography," *Opt. Lett.* **30**(18), 2391 (2005).
23. Z. G. Wang, H. Adler, D. Chan, A. Jain, H. K. Xie, Z. L. Wu, and Y. T. Pan, "Cystoscopic optical coherence tomography for urinary bladder imaging *in vivo*,"*Proc. SPIE* **6079**, 0697905 (2006).

24. Y. T. Pan, T. Q. Xie, C. W. Du, S. Bastacky, S. Meyers, and M. L. Zeidel, "Enhancing early bladder cancer detection with fluorescence-guided endoscopic optical coherence tomography," *Opt. Lett.* **28**(24), 2485–2487 (2003).
25. T. Q. Xie, H. K. Xie, G. K. Fedder, and Y. T. Pan, "Endoscopic optical coherence tomography with a modified microelectromechanical systems mirror for detection of bladder cancers," *Appl. Opt.* **42**(31), 6422–6426 (2003).
26. M. D. Sachs, D. Daniltchenko, E. Lankenau, F. Koenig, G. Huettmann, G. Kristiansen, and S. A. Loening, "Diagnosis and intraoperative staging of bladder disease by *in vivo* optical coherence tomography (OCT)," *J. Urol. (Baltimore)* **171**(4), 68 (2004).
27. Y. T. Pan, Q. Wu, Z. G. Wang, P. R. Brink, and C. W. Du, "High-resolution imaging characterization of bladder dynamic morphophysiology by time-lapse optical coherence tomography," *Opt. Lett.* **30**(17), 2263–2265 (2005).
28. Z. G. Wang, D. B. Durand, M. Schoenberg, and Y. T. Pan, "Fluorescence guided optical coherence tomography for the diagnosis of early bladder cancer in a rat model," *J. Urol. (Baltimore)* **174**(6), 2376–2381 (2005).
29. D. Daniltchenko, M. Sachs, E. Lankenau, F. Koenig, G. Huettmann, D. Schnorr, S. Al-Shukri, and S. Loening, "Optical coherence tomography of the urinary bladder: the potential of a high-resolution visual investigation technique for endoscopic diagnostics," *Opt. Spectrosc.* **101**(1), 40–45 (2006).
30. F. I. Feldchtein et al., "Endoscopic applications of optical coherence tomography," *Opt. Express* **3**(6), 257 (1998).
31. Y. T. Pan, H. K. Xie, and G. K. Fedder, "Endoscopic optical coherence tomography based on a microelectromechanical mirror," *Opt. Lett.* **26**(24), 1966 (2001).
32. J. G. Wu, M. Conry, C. H. Gu, F. Yaqoob, and C. H. Yang, "Paired-angle-rotation scanning optical coherence tomography forward-imaging probe," *Opt. Lett.* **31**(9), 1265 (2006).
33. J. C. Goddard, C. D. Sutton, P. N. Furness, K. J. O'Byrne, and R. C. Kockelbergh, "Microvessel density at presentation predicts subsequent muscle invasion in superficial bladder cancer," *Clin. Cancer Res.* **9**(7), 2583–2586 (2003).
34. D. E. Richard, E. Berra, and J. Pouyssegur, "Angiogenesis: how a tumor adapts to hypoxia," *Biochem. Biophys. Res. Commun.* **266**(3), 718–722 (1999).
35. C. E. Saxer, J. F. De Boer, B. H. Park, Y. H. Zhao, Z. P. Chen, and J. S. Nelson, "High-speed fiber-based polarization-sensitive optical coherence tomography of *in vivo* human skin," *Opt. Lett.* **25**(18), 1355 (2000).
36. Z. Wang, Z. Yuan, H. Wang, and Y. Pan, "Increasing the imaging depth of spectral-domain OCT by using interpixel shift technique," *Opt. Express* **14**(16), 7014 (2006).
37. J. Flamm and S. Dona, "The significance of bladder quadrant biopsies in patients with primary superficial bladder-carcinoma," *Eur. Urol.* **16**(2), 81 (1989).
38. E. M. Messing and W. Catalona, "Urothelial tumors of the urinary tract," in *Campbell's Urology*, 7th ed., P. C. Walsh et al., Eds., pp. 2327–2410, Saunders, Philadelphia (1998).
39. A. R. Tumlinson, J. K. Barton, B. Povazay, H. Sattman, A. Unterhuber, R. A. Leitgeb, and W. Drexler, "Endoscope-tip interferometer for ultrahigh resolution frequency domain optical coherence tomography in mouse colon," *Opt. Express* **14**(5), 1878 (2006).
40. U. Sharma, N. M. Fried, and J. U. Kang, "All-fiber common-path optical coherence tomography: sensitivity optimization and system analysis," *IEEE J. Sel. Top. Quantum Electron.* **11**(4), 799 (2005).